Meteorology of proposed Mars Exploration Rover landing sites

Anthony D. Toigo
Center for Radiophysics and Space Research, Cornell University, Ithaca, New York, USA

Mark I. Richardson
Division of Geological and Planetary Sciences, California Institute of Technology, Pasadena, California, USA

Received 16 February 2003; revised 2 July 2003; accepted 25 August 2003; published 15 November 2003.

[1] A descriptive study of the near-surface meteorology at three of the potential Mars Exploration Rover (MER) landing sites (Terra Meridiani, Gusev Crater, and Melas Chasma) is presented using global and mesoscale models. The mesoscale model provides a detailed picture of meteorology on scales down to a few kilometers but is not well constrained by observations away from the Viking and Pathfinder landing sites. As such, care must be taken in the interpretation of the results, with there being high confidence that the types of circulations predicted will indeed occur and somewhat less in the quantitative precision of the predictions and the local-time phasing of predicted circulations. All three landing sites are in the tropics and are affected by Hadley circulation, by diurnal variations due to the global thermal tide, and by planetary scale topography (in these particular cases from Tharsis, Elysium, and the global topographic dichotomy boundary). Terra Meridiani is least affected by large variations in local topography. Mean winds at Terra Meridiani during MER landing would be less than 10 m/s with little vertical shear. However, these low wind speeds result from strong mixing in the early afternoon convective boundary layer, which creates its own hazard in the horizontal variation of vertical winds of up to 8 m/s (both upward and downward). In Gusev Crater the topography of Ma'adim Vallis and the crater rim generates strong diurnally reversing channeling of wind in Ma'adim Vallis and diurnally reversing radial flow in the crater associated with thermal slope winds on the crater rim. The overturning circulation in Gusev Crater slightly suppresses the daytime convective boundary layer. Melas Chasma in Valles Marineris provides an example of strong topographic forcing of near-surface circulation. Of particular interest is the channeling of regional scale wind toward the center of the Tharsis plateau during the evening. This results in a surface level jet along the canyon of over 25 m/s. Drainage of air from the plateau and into the canyon produces vertical winds down the canyon walls in the evening of over 5 m/s. In contrast, during the early afternoon (MER landing time), horizontal winds at the proposed MER landing site are relatively calm, with little mean shear with height. This results from the proposed site being in a region of local divergence and the action of daytime convection. The nature of flow in Melas Chasma results in an interesting dual maximum in boundary convection and depth, with the usual daytime afternoon free convective maximum being joined by a mechanically forced nighttime boundary layer of almost 2 km depth. *INDEX TERMS:* 5445 Planetology: Solid Surface Planets: Meteorology (3346); 3329 Meteorology and Atmospheric Dynamics: Mesoscale meteorology; 3337 Meteorology and Atmospheric Dynamics: Numerical modeling and data assimilation; 3307 Meteorology and Atmospheric Dynamics: Boundary layer processes; 3344 Meteorology and Atmospheric Dynamics: Paleoclimatology; *KEYWORDS:* Mars Exploration Rovers, mesoscale atmospheric modeling, boundary layer, convection, winds, topographic flows

Citation: Toigo, A. D., and M. I. Richardson, Meteorology of proposed Mars Exploration Rover landing sites, *J. Geophys. Res.*, *108*(E12), 8092, doi:10.1029/2003JE002064, 2003.

1. Introduction

[2] The Mars Exploration Rovers (MER) will touch down on the surface of Mars in January 2004, corresponding to late southern summer. While understanding the meteorology of Mars is not a major scientific goal of the MER mission, meteorology impacts the mission and its results in at least two ways. From an operational perspective, the meteorological conditions at landing sites affects the likelihood of successful landing and the operation of the rovers on the

Copyright 2003 by the American Geophysical Union.
0148-0227/03/2003JE002064$09.00

surface. As a result, the meteorology predicted for the proposed landing sites has played some role in selecting which of the sites the MER rovers are sent to [*Kass et al.*, 2003]. From a scientific perspective, some fraction of the geological features observed and studied by the rovers at any landing site are likely to be aeolian in nature. As such, understanding the near-surface meteorological environment of the landing sites will provide some context for their study. (For a more detailed description of the selection of the landing sites, their location, and their landing ellipses, see *Golombek et al.* [2003] in this issue.)

[3] This paper provides a multi-scale description of meteorology predicted for the MER landing sites through the use of global, mesoscale, and large eddy simulations [*Toigo and Richardson*, 2002; *Toigo et al.*, 2003]. Such numerical models provide the basis for this study as we do not have direct observations for these sites: they have not yet been visited. The models are grounded in extensive terrestrial work [*Dudhia*, 1993], and have been carefully compared with available lander observations [*Toigo and Richardson*, 2002]. In this sense the models allow extrapolation of existing lander data to sites in a physically consistent way. Unfortunately the few data sets which exist for Mars are for relatively flat and featureless locations. One theme of this paper will be the role that topography plays in modifying wind patterns, as discussed for two-dimensional simulations by *Ye et al.* [1990] and *Siili et al.* [1999].

[4] A major problem for assessing the accuracy of the simulations, especially at the mesoscale, is the lack of data available for different types of sites with which to compare and constrain the model (comparison with existing lander data is described by *Toigo and Richardson* [2002]). While it is known that various factors can affect the model simulations (from the nature of the global circulation that provides a boundary condition to the details of the planetary boundary layer parameterization), there is little variational ability to test these sensitivities. The philosophy of this study has been to use the very best global context simulations (as gauged by comparison with global data sets such as those provided by the Mars Global Surveyor Thermal Emission Spectrometer [*Richardson and Wilson*, 2002], and local data sets which reflect global circulation phenomena, such as the Viking and Mars Pathfinder records of diurnal surface pressure cycles [*Wilson and Hamilton*, 1996]) and to examine output from the resulting high-resolution simulations. Assessing the true error in these best-fit cases becomes extremely difficult because of the lack of a reference. Sensitivity, on the other hand, is gauged by varying model parameters and by understanding the influences of global circulation and model parameterizations on the model predictions. In the following sections, we provide some guide as to the confidence the reader can have in various components of the circulation and meteorology predicted for the landing sites. Greater confidence will require more direct observations of diverse locations, and imaginative use of available orbital data.

[5] The diversity of the proposed Mars Exploration Rover landing sites provides a broad spectrum of surface conditions, allowing a variety of interesting meteorology to be examined. In this paper, we will use this motivation to explore: the seasonal and diurnal variation of large-scale wind patterns, the effect of regional and local-scale topography (plateaus, craters, and canyons) upon circulation, the interaction between flows of different length-scales, and the development of convective boundary layers. In the next section, we introduce our modeling approach and the hierarchy of models used. In section 3, we consider the global setting of each landing site, and examine the seasonal and diurnal variations in near-surface wind. The next two sections deal with the mesoscale (hundreds of kilometers) and microscale (tens of meters to thousands of meters) meteorology of the landing sites. Finally, we provide a summary of this study.

2. Modeling Approach and Hierarchy

[6] For the simulation of global-scale process, this study uses the Geophysical Fluid Dynamics Laboratory (GFDL) Mars General Circulation Model (GCM) [*Wilson and Hamilton*, 1996]. This model is additionally used to provide initial and boundary conditions for the mesoscale model simulations. The version of the Mars GCM used here is as described by *Richardson and Wilson* [2002] and *Wang et al.* [2003]. GCM output with a latitudinal/longitudinal grid spacing of 2° by 2.4° is used to examine global scale wind patterns, and to check for consistency between the GCM and mesoscale models (the development of frontal storms in this simulation is described by *Wang et al.* [2003]). The mesoscale initial and boundary conditions are generated from a 5° by 6° simulation. Both simulations employed 20 levels between the surface and 90 km.

[7] The mesoscale model is based on the Pennsylvania State University/National Center for Atmospheric Research (PSU/NCAR) Mesoscale Model Version 5 (MM5) [*Dudhia*, 1993]. The conversion to Mars, included processes and surface boundary condition data sets, and validation of this model is described by *Toigo and Richardson* [2002]. The MM5 has also been converted to Mars independently by *Tyler et al.* [2002]. The implementation of the Mars MM5 used in this study is non-hydrostatic and employs GFDL Mars GCM simulations for initial and boundary conditions. Multiple embedded model domains (or nests) are used to bridge between the GCM grid spacing (approximately 300 km) and that of the best-resolved MM5 domain (1 km). The MM5 has been modified to allow slightly larger ratios of nest-to-parent domain ratios (from 3 to 5 [cf. *Toigo and Richardson*, 2002]); thus we will show nests at 1 km, 5 km, 25 km, and 125 km grid spacing. The last of these is very similar to the 2° by 2.4° GCM simulation. The vertical resolution in all domains is approximately 10 m in the lowest layer, increasing to about 200 m toward the model top.

[8] A third model type used in this study is simply a modified version of the MM5, designed to allow direct simulation of turbulence in the boundary layer [*Toigo et al.*, 2003]. This "Large Eddy Simulation" (LES) model (where the terminology has been directly taken from the terrestrial literature [e.g., *Stevens and Lenschow*, 2001]), is used to simulate motions on scales of 100 m. The LES used in this study does not take boundary conditions. Instead, it is uses periodic or cyclic boundary conditions which allow any features advected out of one side of the domain to reenter from the other. This model is used to examine the nature of the convective boundary layer, which is the dominant

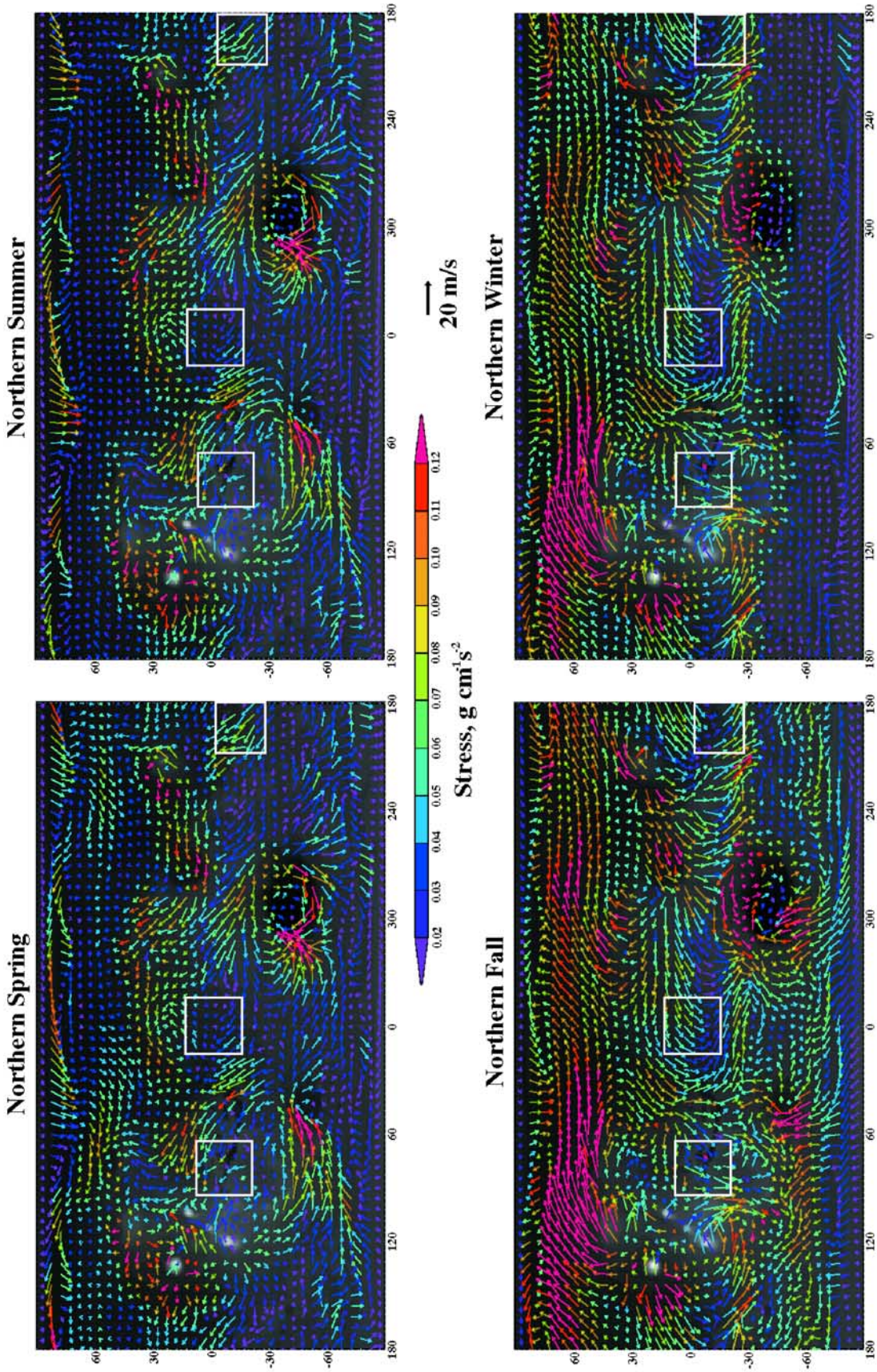

Figure 1. Diurnally and seasonally averaged near-surface (approximately 150 m) winds predicted by the GFDL Mars GCM. Winds are an average over the full diurnal cycle and the full 90° of L_s for each of the seasons indicated. Wind vectors are colored by the strength of their predicted wind stress. White boxes show the regional domains used to predict meteorology at three of the proposed MER landing sites. Figure derived from *Fenton and Richardson* [2001].

concern for the relatively flat Terra Meridiani (''Hematite'') site. The modifications to the MM5 necessary for it to undertake LES runs are described by *Toigo et al.* [2003].

[9] All of the models described in this paper employ essentially the same physical parameterizations. Specifically, the models employ visible and infrared band radiative heating models for CO_2 and dust, and treat dust as a transportable and radiatively active trace species. Dust is injected into the lowest model layer based on near-surface static stability. The model injection rates have been tuned to reproduce global mean and global thermal tide infrared observations [*Wilson and Richardson*, 2000; *Richardson and Wilson*, 2002]. While not of significance for this study, the models also include active CO_2 condensation/sublimation parameterizations, and representations of the phase change and transport of water [*Richardson and Wilson*, 2002; *Toigo and Richardson*, 2002].

3. Global and Synoptic Setting

[10] The near-surface wind patterns and their variation over seasonal and diurnal cycles have been addressed on the global scale or synoptic scale (with a resolution of 5° or lower) by *Greeley et al.* [1993] and *Fenton and Richardson* [2001]. Substantial seasonal and diurnal variability exists in the tropical latitudes available to the MER landing system due to the activity of thermal tides and the seasonally reversing Hadley circulation. The tides generate a tropical surface wind pattern with strong convergence trailing the subsolar point in longitude, and with divergence located roughly 180° of longitude or 12 hours of local solar time behind the daytime convergence. The Hadley circulation is strongly modified by the tidal flow, but has a daily-mean surface flow that traces an arc from the winter to the summer tropics. The arc is toward the west in both seasons, due to the effects of planetary rotation on the flow. The pattern of surface winds exhibit spatial variability independent of these temporal effects due to the large variation in zonal topography. Where highlands, such as the Tharsis plateau, generate obstacles in the zonal direction, the Hadley circulation low-level flow can be modified (concentrated) to form western boundary currents analogous to those operating in the terrestrial ocean basins [*Joshi et al.*, 1995]. Thus, even after accounting for the tidal flow, the Hadley cell surface level wind field is far from zonally uniform. Further local deviations from these synoptic scale patterns are likely when the atmosphere is examined at higher resolution, due to the influence of local and regional (mesoscale) topography. These factors will be discussed in sections 4–6.

[11] The seasonal- and diurnal-average near-surface (approximately 150 m) winds generated by a 5° by 6° version of the GFDL Mars GCM are shown in Figure 1, which is modified from Figure 1 of *Fenton and Richardson* [2001]. The three main candidate sites examined in this paper are indicated by white boxes. The figure shows that the Gusev Crater and Terra Meridiani sites are embedded in relatively unmodified Hadley cell return flow. In northern spring and summer, the Terra Meridiani site exhibits weak but clear northward flow, with an arcing trend from southeasterly (i.e., from the southeast) in the south of the box to southwesterly in the north. The Gusev Crater region exhibits stronger mean winds during these seasons, but without the arcing pattern, presumably due to the influence of nearby Tharsis and Elysium. The southeasterly winds are significantly stronger than at Terra Meridiani and more uniform in direction. In southern spring and summer, the mean wind patterns reverse in the sense expected for mean Hadley cell-like flow. The tendency for predominant mean winds to blow along the northwest-southeast axis at all seasons in the model agrees well with the observed trend of large-scale dark streaks in Gusev Crater (Figure 2). Both the Terra Meridiani and Gusev Crater regions exhibit strong, net southward motion, with flow arcing from northeasterly in the north of the boxes to northwesterly in the south.

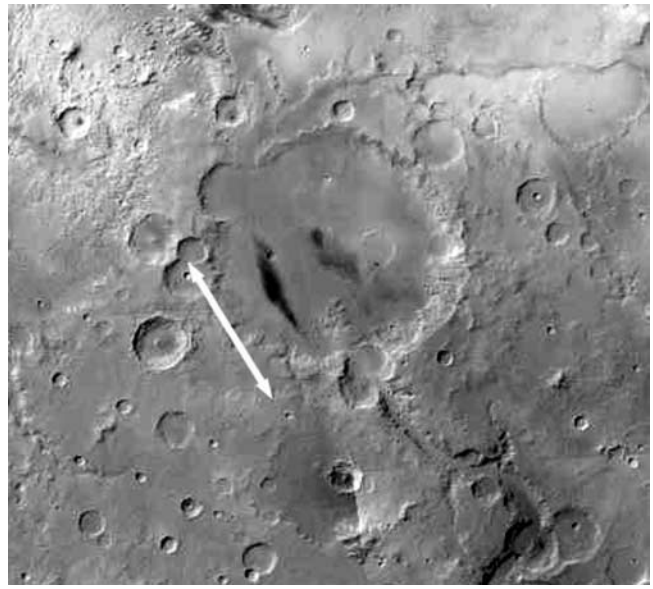

Figure 2. Mosaic of Mars Orbiter Camera (MOC) wide angle images showing a dark streak in the basin of Gusev Crater. The orientation of this streak agrees well with the GCM-predicted winds at this location in local spring and summer seasons.

[12] The Melas Chasma region, in the center west of Valles Marineris shows strong modification of the mean winds by Tharsis. At the model resolution, Valles Marineris itself is not resolved, so the observed modification is associated with the regional topography of the plateau. In northern spring and summer, there is little net flow across the Melas Chasma region, which sits to the west of a strong northward current in Acidalia-Chryse. In southern spring and summer, the Melas Chasma region becomes dominated by generally north-northeasterly flow, which appears to be a strongly modified component of the southern spring and summer Hadley cell return flow.

[13] The variation of the regional wind patterns with local time for the MER landing season (late southern summer) is shown for the three landing site regions in Figures 3 (Terra Meridiani), 4 (Gusev Crater), and 5 (Melas Chasma). Output from the 2° by 2.4° GCM simulation is shown along with the lowest-resolution mesoscale model nest (driven by GCM boundary conditions from the 5° by 6° simulation). These figures show the local time modulation of the winds, which involves full rotation of the wind

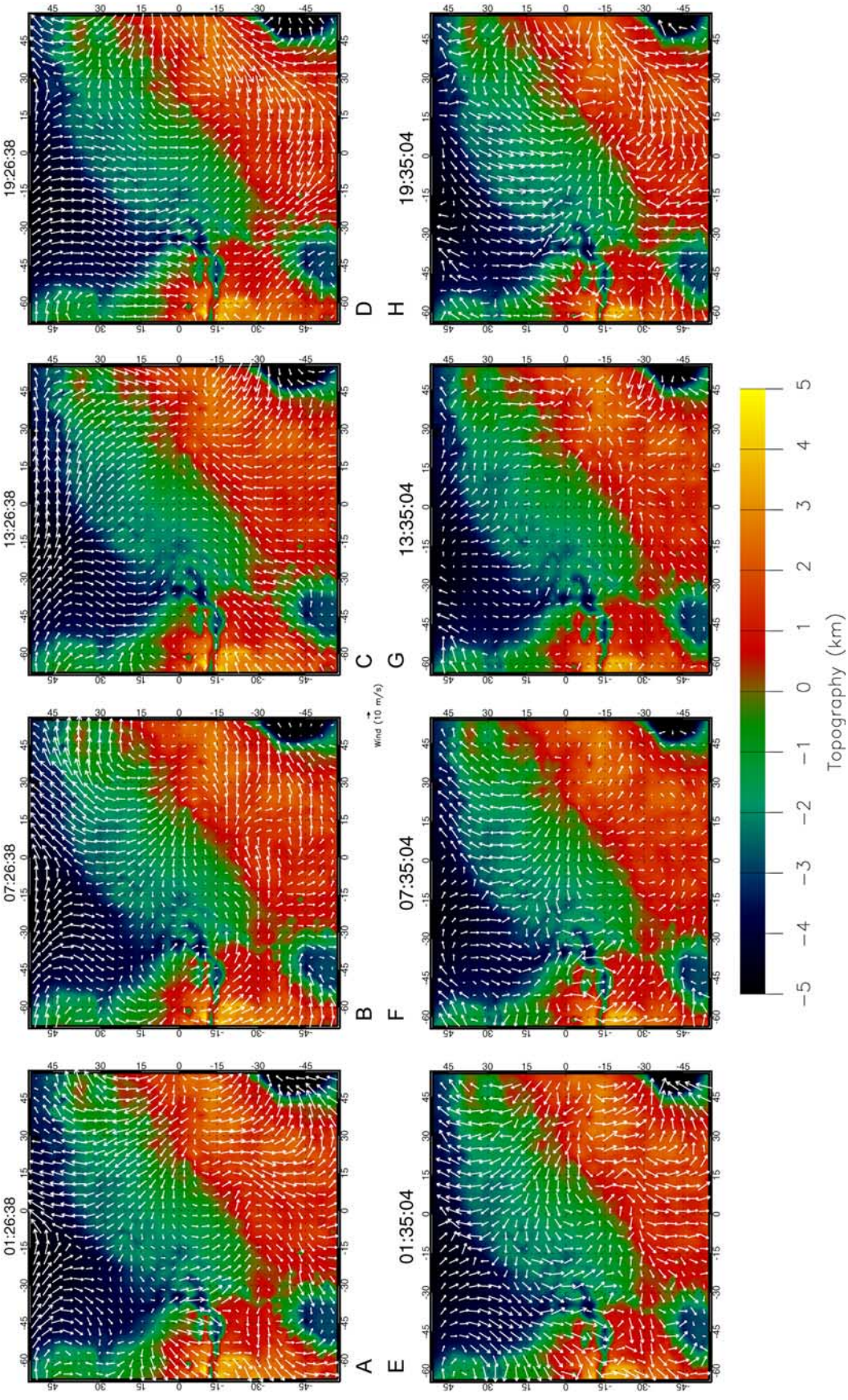

Figure 3. Near-surface winds (approximately 150 m from the surface) from both the coarsest-resolution (Δx = 125 km) mesoscale model simulation (A–D) and the 2° by 2.4° GCM simulations (E–H) for the Terra Meridiani region. Four local times are plotted for each case, separated by 6 hours, and correspond to the local time at the center of the plotted region. (A) and (E): 0130 LT, (B) and (F): 0730 LT, (C) and (G): 1330 LT, and (D) and (H): 1930 LT. Background colors show local topography, with a color scale indicated below, and a scale arrow for the wind vectors is shown in the center. Note that the mesoscale model winds are slightly smoother than the GCM model winds due to the need for slightly higher horizontal diffusivity in the mesoscale model for numerical stability.

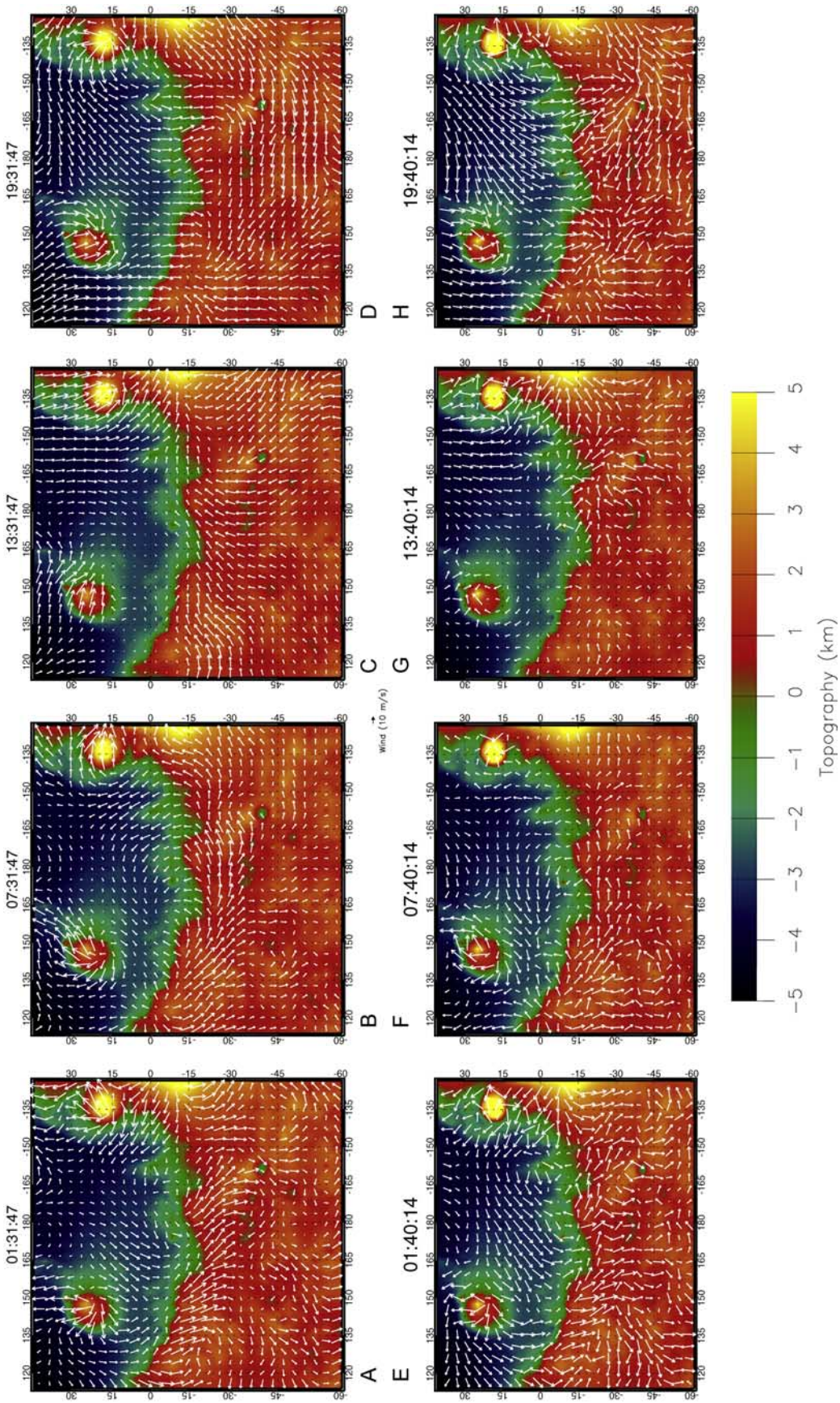

Figure 4. Same as Figure 3, except for the Gusev Crater region.

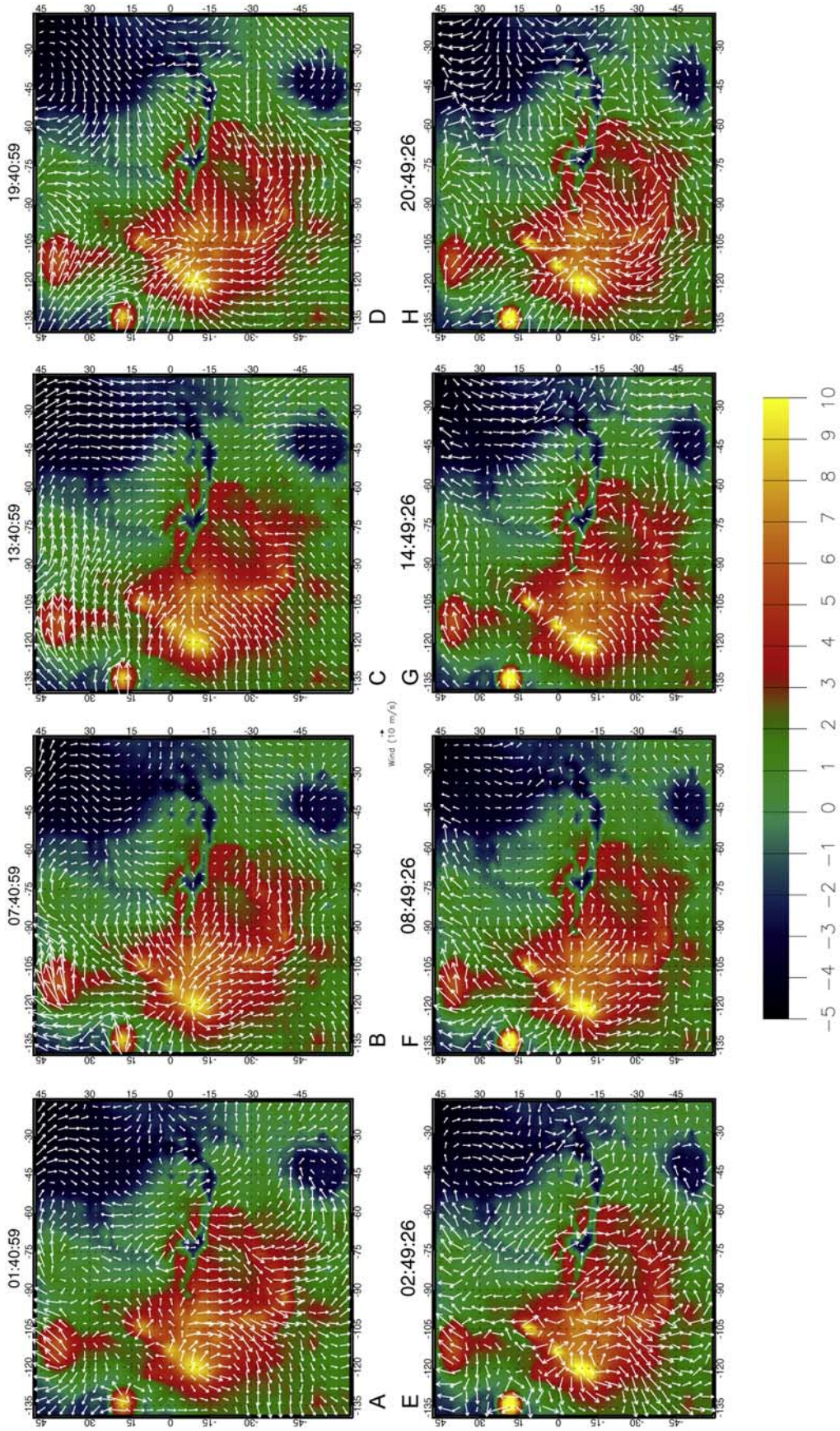

Figure 5. Same as Figure 3, except for the Melas Chasma region.

vectors at many sites over the course of the daily cycle. When averaged over the full diurnal cycle the flow in these regions is similar to that shown in Figure 1.

[14] The strong influence of topography on the near-surface wind is clearly illustrated in Figures 3–5. In the Gusev Crater region (Figure 4), the topographic dichotomy boundary provides a break in the strength and direction of flow at most local times; Elysium is seen to be associated with its own, slope-driven circulation; and, the edge of the Tharsis plateau on the east of the domain presents a distinct break in the wind patterns. In the Terra Meridiani region (Figure 3), the southern highlands form a very large "ridge" between Chryse and Argyre. This ridge acts as a focus for local daytime flow and hence convergence due to regional-scale slope flow. Even in the lowest-resolution mesoscale simulation and the 2° GCM simulation, regional topography on scales down to a few hundred kilometers are seen to have the potential for important impact on the surface wind patterns.

[15] The GCM is the best constrained of the models, as large amounts of global thermal and imaging data, and lander tidal pressure data (which provide information on global wave systems) are available and have been used [*Wilson and Hamilton*, 1996; *Wilson and Richardson*, 2000]. Of most import for this paper, the surface wind directions have been tested against surface wind streak data [*Fenton and Richardson*, 2001], with very good agreement in most areas. Greatest error was encountered in regions of large topography, primarily the Tharsis plateau and volcanos. The error can be significant in direction. Comparison is made difficult in these locations as the streak data can be strongly influenced by local topography on scales barely or not resolved by the model.

4. Terra Meridiani ("Hematite Region")

[16] The mean-flow, near-surface winds at the Terra Meridiani site are dominated by the interaction of regional-scale (topographically forced) and synoptic scale flow, with little change in the flow occurring as model grid spacing is reduced below 125 km. Thus, akin with the Viking and Pathfinder Landing sites, large-scale models including higher-resolution GCMs would likely be able to do a good job in modeling near-surface winds at the Terra Meridiani site, were any data to be collected. The wind speeds and directions predicted at the center of the best resolved domain (corresponding to the center of the MER landing ellipse) and for 5 m above the surface are shown in the form of a hodograph in Figure 6. Peak winds occur in the late evening (2000 Local Time or LT) at about 13 m/s from the northwest. By early afternoon (1330 LT), near the MER landing time, the winds have rotated to southerly to southeasterly with speeds of about 4.5 m/s. The strength of mean surface winds at the Terra Meridiani site should not be of concern to the safety of the MER landing system. Wind speeds less than 15 m/s are considered safe for the landing system [*Golombek et al.*, 2003].

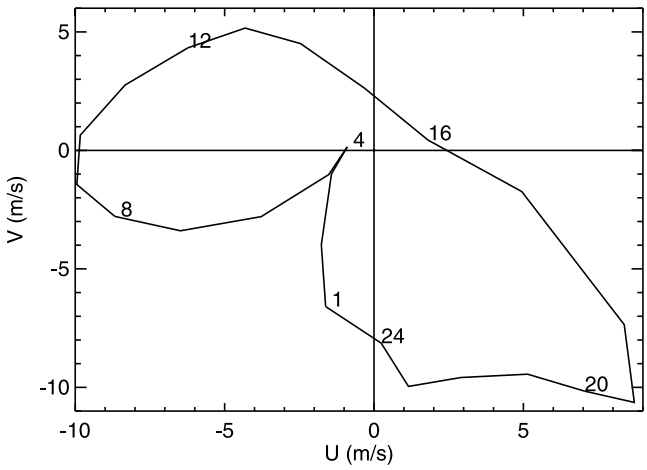

Figure 6. Hodograph of the near-surface (approximately 5 m from the surface) winds at the Terra Meridiani landing site. The plotted line shows the predicted wind magnitude and direction as a function of local time of day, indicated by the numbers around the line. Data come from the highest-resolution (Δx = 1 km) simulation.

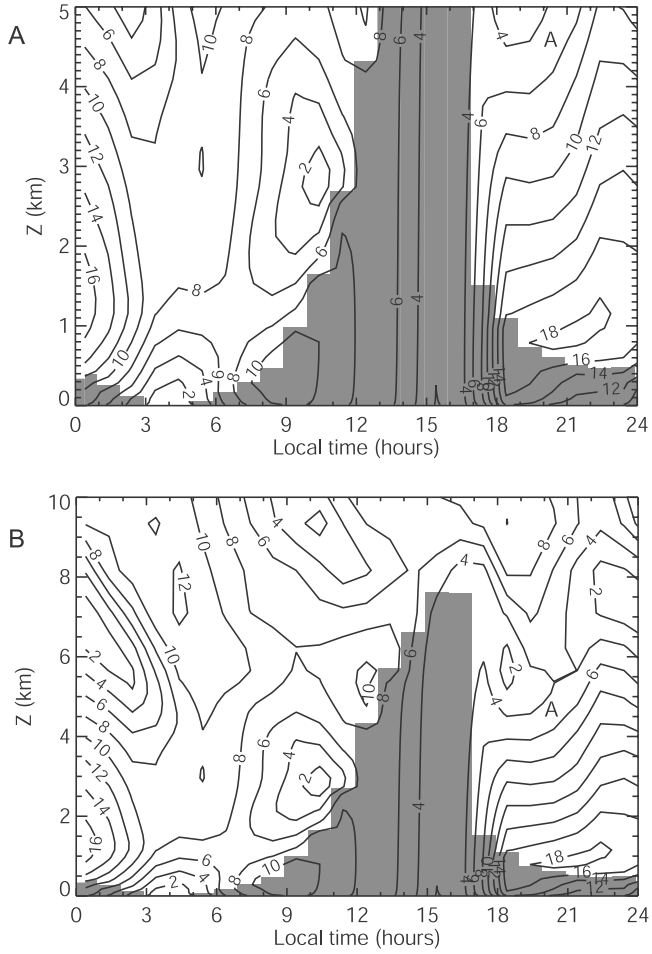

Figure 7. Plot of total horizontal wind speed as a function of local time of day and height at the proposed Terra Meridiani landing site from the 1 km horizontal resolution domain. Wind speed is contoured in units of m/s, and the gray shading shows the Mars MM5-predicted height of the boundary layer as a function of time of day. The only difference between (A) and (B) is the upper height of the plot, 5 km in (A) and 10 km in (B).

[17] The variation of total wind with height and local time at the center of the landing ellipse is shown in Figure 7. The boundary layer height predicted by the Mars MM5 planetary boundary layer (PBL) parameterization is also shown. At night, a maximum in wind speed develops at about 1 km above the surface as the daytime boundary layer collapses. This jet attains a speed just above 18 m/s. Winds decay in the early morning before building again to a morning maximum of just over 10 m/s at 0900 LT. Shortly thereafter, the convective boundary layer begins to develop, efficiently mixing momentum in the vertical. The convective PBL expands to a maximum height of about 7.5 km by 1500 LT, with uniform winds of about 4 m/s throughout. By virtue of an early afternoon landing, the MER rovers will encounter a mean atmospheric wind profile that is rather uniform, with little in the way of horizontal wind shear, and relatively benign mean wind speeds.

[18] There is a big "however" to that statement that is a consequence of landing during the period of strong PBL convective activity. The process that mixes mean horizontal wind in the vertical involves small scale three-dimensional circulations that constitute the PBL convection. Typical vertical and horizontal winds at mid-level in the PBL at roughly 1350 LT are shown in Figure 8. The circulation at this time is composed of irregular convective rolls and open cells. The rolls are aligned roughly parallel with the mean wind in structures that are analogous to those behind convective roll clouds or cloud streets [e.g., *Stull*, 1988]. While perturbation horizontal winds at these levels are not high (a maximum of approximately 4 m/s, though these perturbation winds should be applied to a mean wind of over 4 m/s, yielding net horizontal winds varying from 0 to over 8 m/s), vertical winds in the updrafts can exceed 9 m/s, with the broader downdrafts showing speeds of up to 7 m/s. The width of individual updrafts is roughly 1 km, with horizontal shear of vertical winds being about 16 m/s over a distance of approximately 2 km.

[19] The dominant circulation components in Terra Meridiani are the large-scale, topographically and tidally modified Hadley circulation and the local-scale boundary-layer convective motions. Very high confidence can be placed in the occurrence of each of these systems and their gross phasing (the convection will occur in the daytime as opposed to night time). The mean surface winds could be in error by a factor of two or so due to various errors in the model (calculations of boundary layer diffusivity, mainly) based on our experience modeling the Viking and Pathfinder landing site data [*Toigo and Richardson*, 2002]. The scale and vigor of the daytime convection is also much more prone to error than is the prediction of local time phasing, which is strongly controlled by the passage of the subsolar point. The scales of our cells produce a roughly unit aspect ratio, and a PBL depth of about 7 km, the latter of which is roughly consistent with simpler PBL models [*Haberle et al.*, 1993]. The unit aspect ratio is consistent with terrestrial experience [*Willis and Deardorff*, 1979]. While the model resolution in LES mode is much finer than the scale of these structures (100 m versus 7 km), it is possible that finer-scale convective structures are being smoothed. The fact that a finite horizontal diffusivity must be used in the model for numerical stability may also reduce the effectiveness of the model in capturing finer scales. While the predicted aspect ratio and PBL height have a solid basis in terrestrial analog and simpler modeling of the Martian PBL, the convective wind speeds predicted by the model are less well constrained. Again, we feel that an error of a factor of two or so is appropriate, but this is more difficult to support in this case. Some confidence is gained from the fact that the model is able to generate dust devils with central pressure drops and wind speeds similar to those observed [*Toigo et al.*, 2003].

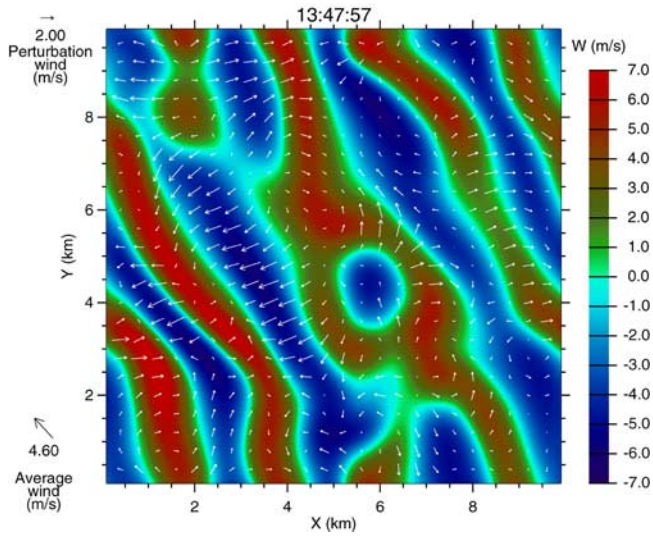

Figure 8. Upward wind (w) at approximately 1.4 km above the surface overlaid with white arrows showing the perturbation horizontal wind at that height from the Terra Meridiani large eddy simulation. Perturbation winds are the instantaneous wind subtracted from the average wind at this level. The average wind vector for this level is plotted at the lower left. Note that one in every 16 wind vectors is plotted (one in every four in each Cartesian direction).

5. Gusev Crater

[20] Gusev Crater, Ma'adim Vallis, and nearby Apollinaris Patera present topographic structures which impact the nature of the near-surface wind pattern in this region. Unlike at the Terra Meridiani site, winds predicted by a moderately high-resolution GCM would not do a good job of predicting in-situ mean winds for a large fraction of the Gusev Crater study region. To emphasize this, Figure 9, which shows the near-surface wind patterns in the 5 km and 25 km grid-spacing domains, should be compared with Figure 4. While the effects of the dichotomy boundary and the strong, diurnally varying slope flow on Elysium are captured by the GCM, there is little in the way of perturbed flow near Gusev. However, the 25 km domain shows that Apollinaris Patera, just north of Gusev, generates a significant local wind system of daytime upslope flow and strong nighttime drainage winds. The 5 km grid provides a good picture of the influence of Ma'adim Vallis and the crater itself upon the flow.

[21] Ma'adim Vallis acts as a strong wind conduit, producing diurnally reversing winds that flow locally along the valley. Rotation of the winds occurs due to variations in surface pressure gradients associated with the global-scale

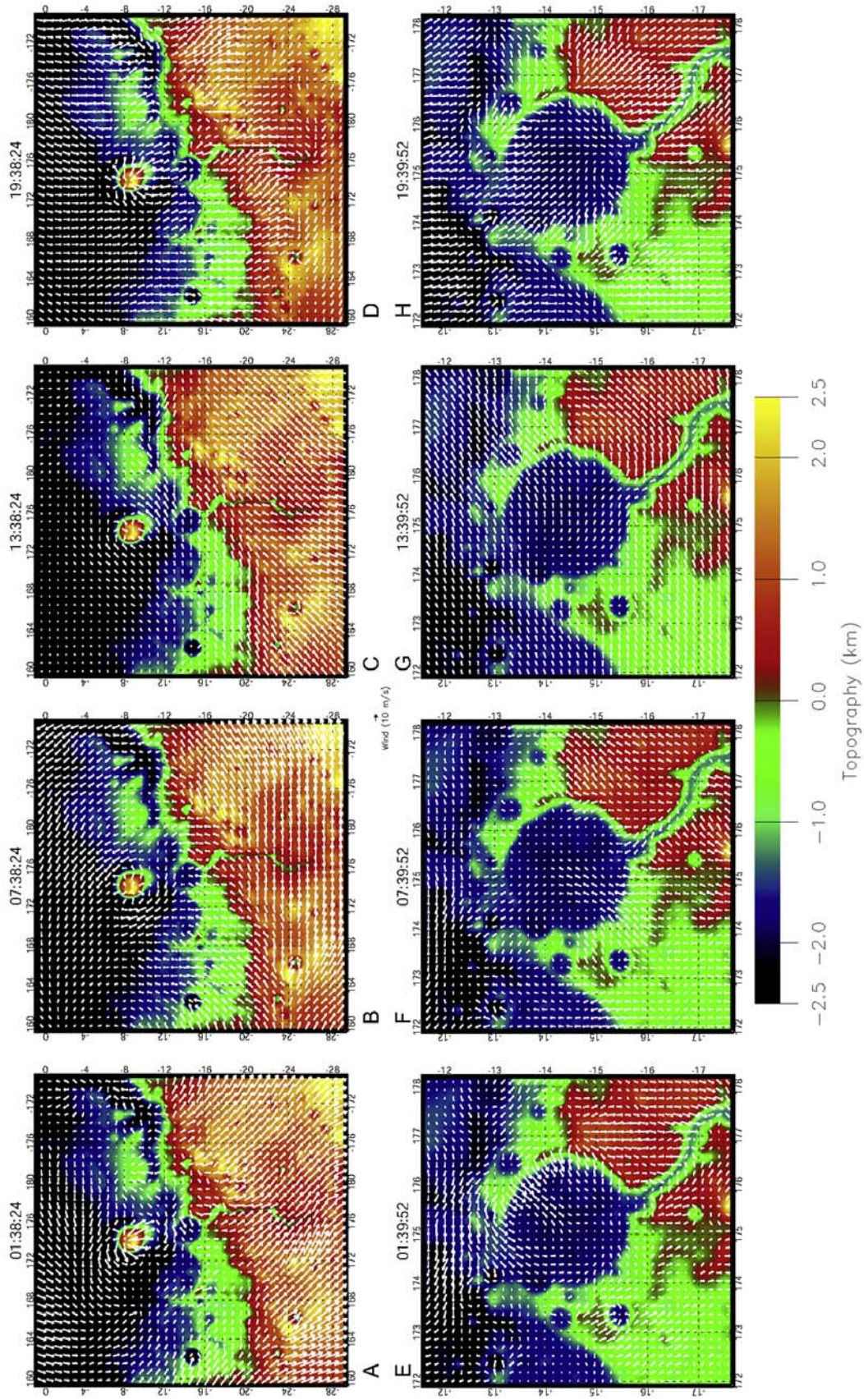

Figure 9. Near-surface winds (approximately 5 m from the surface) from both of the medium-resolution mesoscale model simulations for the Gusev Crater region. (A)–(D) show the $\Delta x = 25$ km simulations (with Gusev Crater at center just south of Apollinaris Patera), and (E)–(H) show the $\Delta x = 5$ km simulations. Four local times are plotted for each case, separated by 6 hours, and correspond to the local time at the center of the plotted region. (A) and (E): 0140 LT, (B) and (F): 0740 LT, (C) and (G): 1340 LT, and (D) and (H): 1940 LT. Background colors show local topography, with a color scale indicated below, and a scale arrow for the wind vectors is shown in the center.

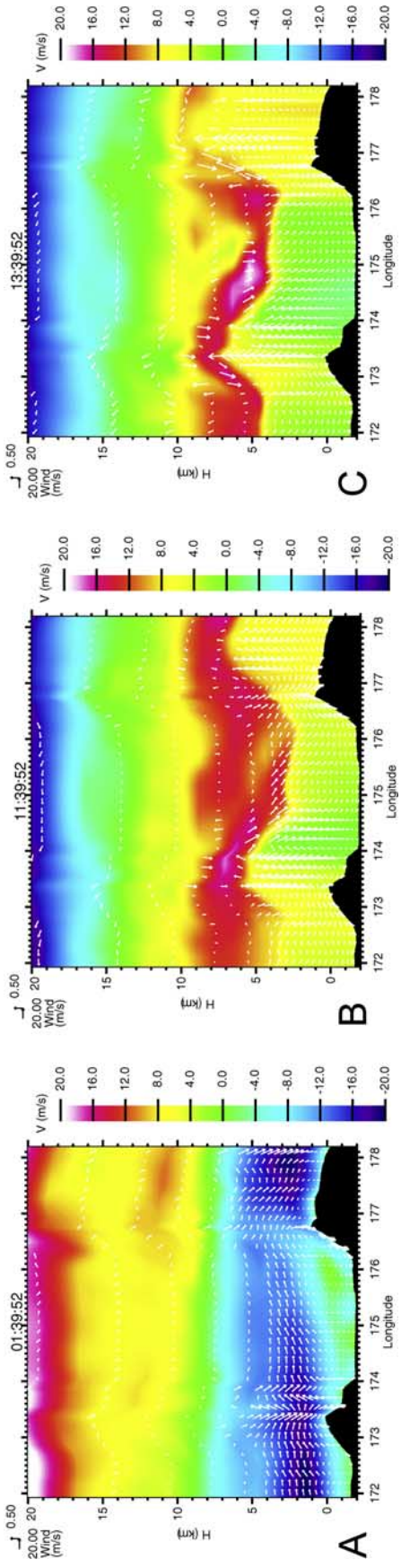

Figure 10. Winds over Gusev Crater at three sample local times of day, from the $\Delta x = 5$ km simulation. The plane shown is east-west by vertical, and longitude is labeled. Background colors show the magnitude of the north-south (u) wind, and the wind vector arrows show the magnitude of the east-west and up-down winds. Since the vertical winds are much weaker than the horizontal winds, they have been exaggerated by a factor of approximately 40 relative to the horizontal component. Scale arrows for each direction are show at the upper left of the figure. (A) 0140 LT. (B) 1140 LT. (C) 1340 LT.

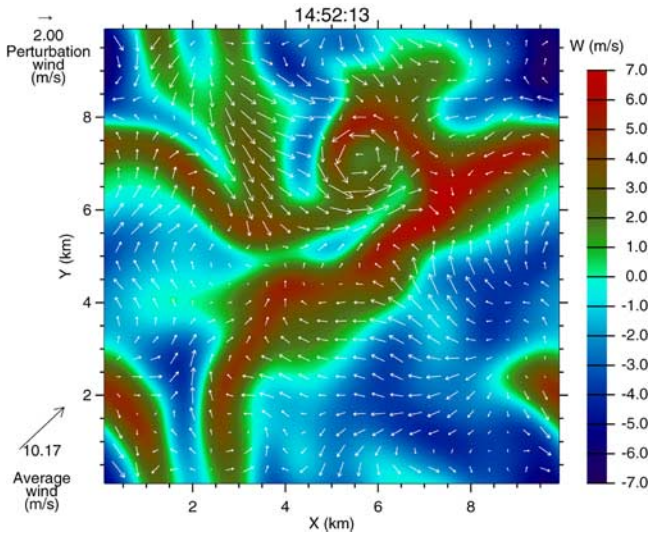

Figure 11. Same as Figure 8, except for the Gusev Crater large eddy simulation.

tide and with more local, thermal/topographical forcing. In the post-sunrise morning, flow is into the valley and then along the channel, disgorging in the crater. At most other local times, flow is out of the crater. In the afternoon, the relatively high and level ground to the south of Gusev (and into which Ma'adim Vallis is cut) is uniformly covered with westerly to northwesterly winds. These winds flow into the valley on its western side, and out on its eastern side. The flow in the valley itself remains aligned along the valley. Mars Orbiter Camera images have shown examples of such

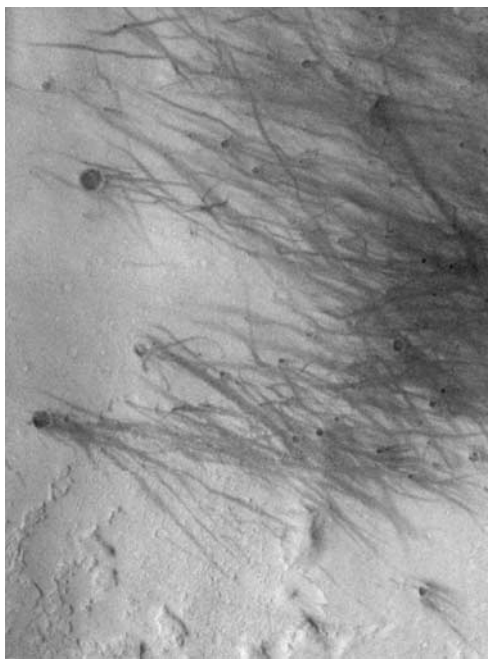

Figure 12. Portion of THEMIS visible-wavelength image frame number V00881003 showing dust devil trails on the floor of Gusev Crater. The image is centered at approximately 14.5°S and 175.5°E, and shows an area approximately 15 km by 10 km.

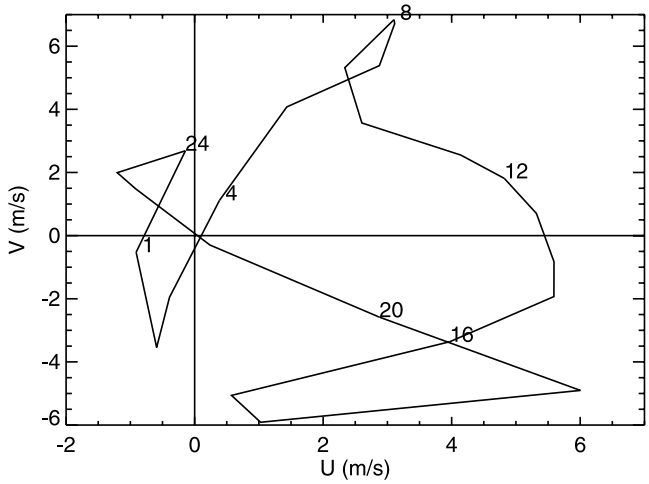

Figure 13. Same as Figure 6, except for the Gusev Crater proposed landing site.

variations in wind direction recorded in differing orientations of dunes on plateau surfaces versus those in channels cut into the plateaus [*Malin and Edgett*, 2001].

[22] Gusev Crater generates a diurnally varying wind system through slope winds that develop on the crater

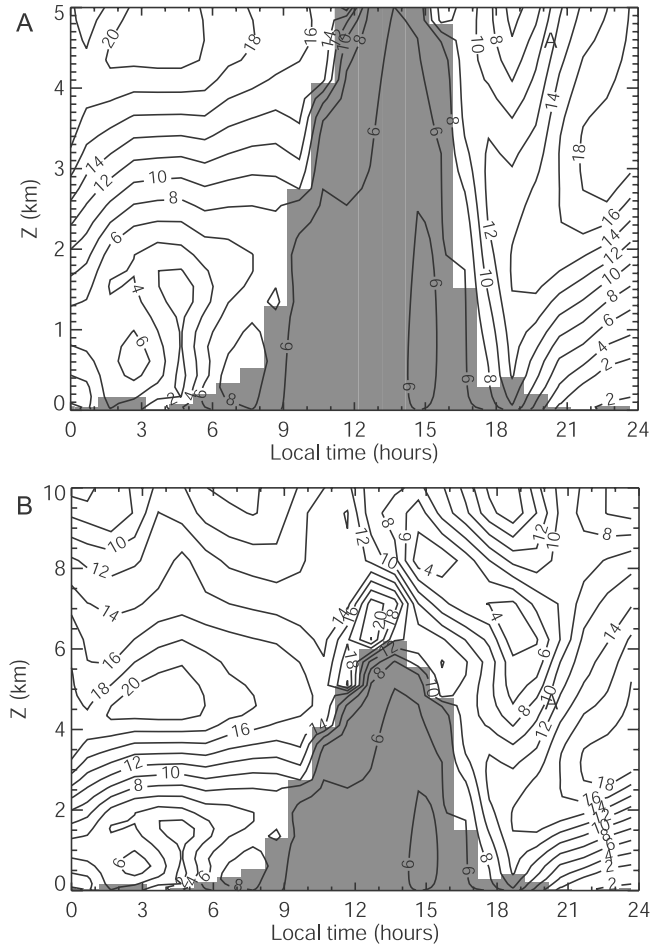

Figure 14. Same as Figure 7, except for the Gusev Crater proposed landing site.

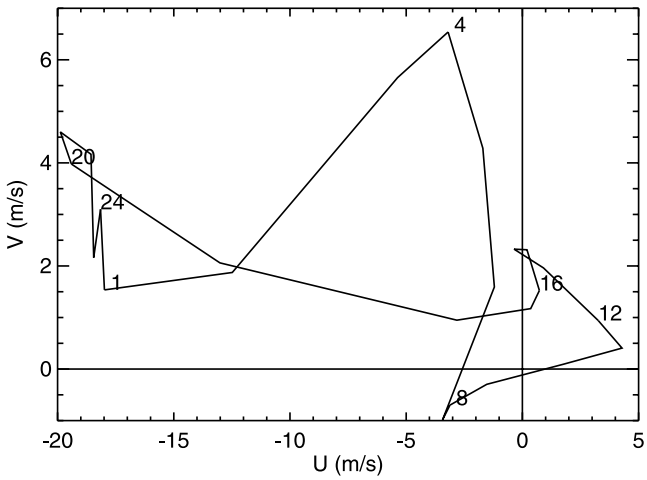

Figure 15. Same as Figure 6, except for the Melas Chasma proposed landing site.

rim. During the evening and night, cooling of air on the top of the rim generates dense air which flows radially into the crater. During the mid-day, heating over the crater rim generates upwelling plumes and consequent flow up the crater rim. This system is seen as a radial inflow-outflow pattern superposed upon the regional flow patterns. The three-dimensional nature of this crater slope flow is further illustrated in Figure 10, which shows cross sections through the 5 km grid domain in the early morning and around noon. Figure 10a shows the shallow (3–5 km) cell that develops as a result of crater drainage flow on the eastern rim. These surface winds on the rim exceed 20 m/s, with more than a 1 m/s vertical (downward) component. Downward flow on the western crater wall is muted by the mean westerly winds near 3–5 km above the surface. This wind tends to induce a whole-crater overturning circulation which reinforces the downslope flow on the eastern wall and opposes it on the western crater wall. Figures 10b and 10c show the development of upwelling plumes over the crater walls near noon.

[23] Turbulence in the daytime convective boundary layer occurs above the Gusev crater floor in a manner analogous to the Terra Meridiani site. A sample of a LES run for Gusev Crater is shown in Figure 11, showing amongst other things the development of a vertical vortex. Mars Orbiter Camera (MOC) and Thermal Emission Imaging System (THEMIS) images show evidence of dust devil activity in Gusev Crater in the form of dust devil streaks (Figure 12). The perturbation horizontal winds are up to 3 m/s at mid-levels, with vertical winds ranging between 7 m/s up and down. These perturbation winds are superposed upon mean winds of approximately 6 m/s in the early afternoon (the diurnal variation of near-surface winds is shown in Figure 13 for Gusev Crater).

[24] The depth of the convective boundary over the Gusev crater is shown in Figure 14. The maximum PBL depth here is over a kilometer and a half lower than at Hematite. The difference in height is not associated with the energetic drive for convection. Instead, the boundary layer is suppressed by mean downwelling over the crater during the early afternoon. Circulation resulting from thermal slope wind upwelling over the crater rim is closed by downwelling over the center of the crater. This downwelling increases in the afternoon, causing the PBL depth to decrease after 1300 LT, in contrast with the expectation that the PBL will deepen until the late afternoon (for comparison the Terra Meridiani PBL depth increases until after 1700 LT; see Figure 7).

[25] The Gusev Crater mesoscale and LES simulations are subject to similar patterns of confidence and uncertainty as those for the Terra Meridiani. Some additional uncertainty exists due to the importance of slope wind systems. The general phasing of the slope wind systems should be accurate to 2 to 3 hours or better, as they depend strongly on the diurnal cycle of insolation. The wind speeds within the crater system depend upon the interaction of the large scale circulation, the crater-scale topographically forced circulation, and the PBL convection. As such, there could be significant error at any given location within the crater due to modest errors in the relative intensity and location of these interacting systems. Again, the mean winds at low levels will be slowed by the drag induced by PBL daytime convection, and therefore significant confidence can be placed in the prediction that the wind speeds below about 5 km altitude will be significantly lower than those above that level (above the top of the PBL) on the floor of the crater.

6. Melas Chasma (Valles Marineris)

[26] The Tharsis Plateau strongly modifies atmospheric circulation by presenting an obstacle to flow which would occur in its absence, and by generating extensive regional scale slope wind systems (Figure 5). The global tidal circulation and large scale slope winds combine to generate large scale flow toward the center of Tharsis (and particularly toward the volcano summits) during the daytime, but lagging noon by a few hours. At night, the same components combine to yield strong flow away from the plateau center. As the tidal convergence point moves over the plateau, strong winds at a tangent to the plateau center develop, first to the east and later in the day to the west. These regional winds provide the boundary conditions, or the backdrop, for the flow that occurs within Valles Marineris.

[27] The hodograph for the center of the Melas Chasma landing ellipse (Figure 15) shows that the primary variation of near-surface winds in this portion of the canyon is between strong along canyon flow (to the west-northwest in the late evening to midnight) and stagnant to slightly reversed flow (in the late morning). The nighttime flow develops substantial speeds, in excess of 20 m/s. The hodograph suggests wind flow that is consistent with expectation: the deep canyon system tends to channel wind along its long axis.

[28] The relationship between along canyon flow and the Tharsis regional circulation is shown in Figure 16. In the early morning, the regional flow is away from the center of the plateau and generally toward the east both north and south of the canyon. At the rim of the canyon, winds are generally perpendicular to the walls, directed into the canyon, with significant velocities (about 15 to 20 m/s) on the northern wall. In Figure 16a, it can be seen that flow is into all of the various canyon sections, generating strong

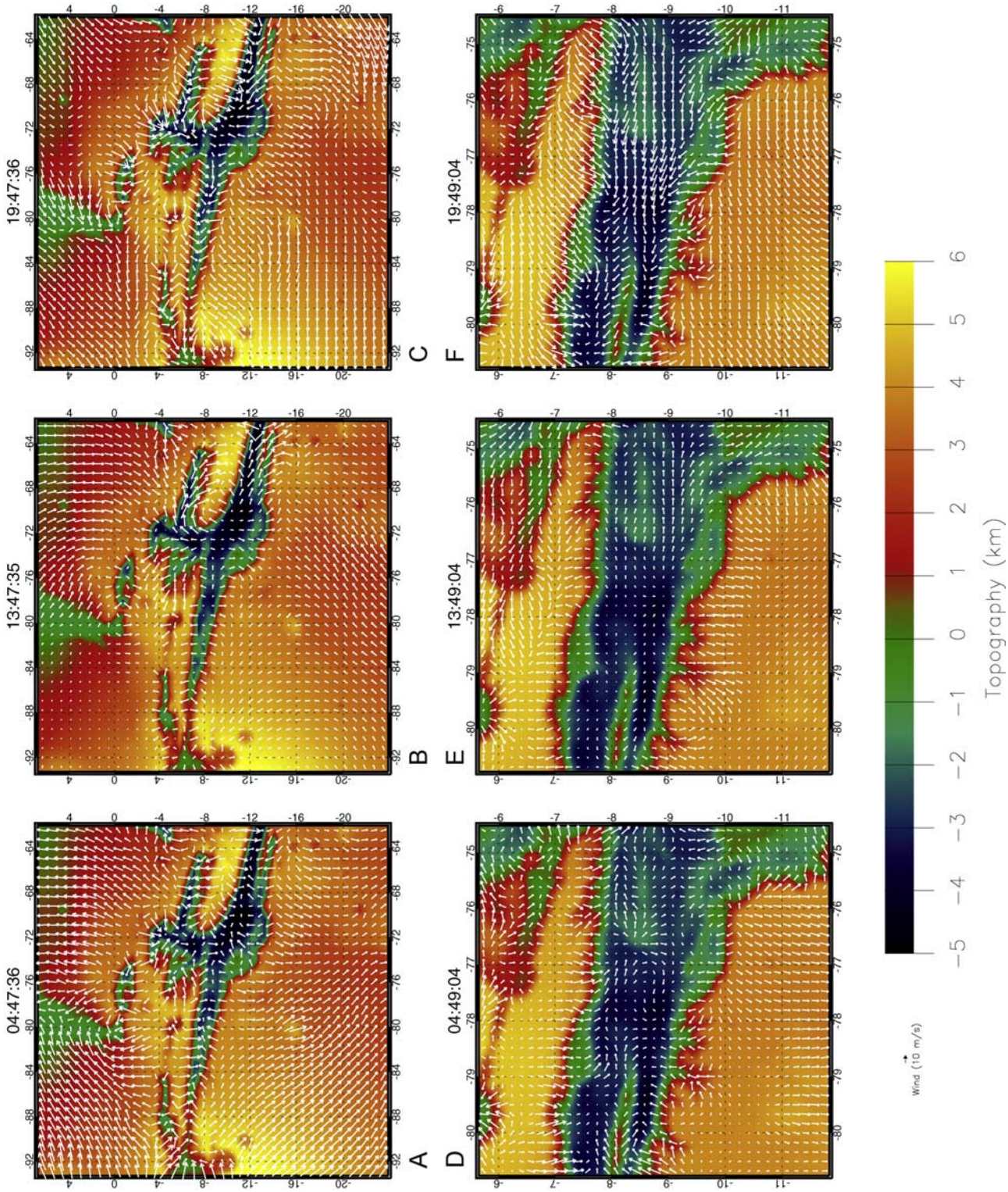
04:47:36
13:47:35
19:47:36
04:49:04
13:49:04
19:49:04
A
B
C
D
E
F
Wind (10 m/s)
Topography (km)
6
5
4
3
2
1
0
−1
−2
−3
−4
−5

divergence on the section of plateau dividing Coprates Chasma from Candor Chasma. Looking at Melas and Ius Chasma at higher resolution (Figure 16d), details of local flow into the main canyon through "tributary" canyons can be seen, with the density currents efficiently seeking out the maximum local downhill gradient.

[29] By early afternoon, the regional flow turns around to flow up the plateau toward higher elevations (Figure 16b). Convergence in the regional flow at this time occurs toward Valles Marineris. However, close to the canyon, flow is strongly divergent as a result of strong slope winds up the canyon walls. This strong canyon slope flow generates strong surface winds in Candor Chasma. However, in Melas and Ius, the surface winds are very calm near the landing site (Figure 16e). To the east of the landing site, winds flow from Melas toward the central junction of Valles Marineris. To the west, gentle flow up the canyon to the west occurs. The landing site itself is in the stagnant divergence point between these surface flows.

[30] By late evening, the regional flow on the plateau is strongly to the west, due mainly to the tidal circulation (Figure 16c). This flow is roughly aligned with the axis of the canyon, and strong along canyon flow develops throughout the whole of Valles Marineris. In addition to the along canyon flow, the cooling of air on the plateau following sunset again generates strong flow down the canyon walls (Figure 16f). The landing site is now located in a position of amplified surface level flow as the canyon contracts just to the west.

[31] A cross section through the three-dimensional circulation at the landing site longitude is shown in Figure 17 for the three local times shown in Figure 16. In the early morning (Figure 17a), strong drainage flow into Melas and Ius Chasma is evident on both walls of the canyon, with the flow on the northern wall being the strongest (over 10 m/s vertical speeds). Drainage on the southern wall (which is consequently flow to the north) is diminished by the relatively strong southwestward flow on the plateau just south of the canyon. The larger-scale plateau flow at this time is toward the east, and as a result there develops flow in the canyon with a net eastward component. This flow is strongly concentrated along the northern wall of the canyon and at about 500 m to 1 km above the canyon floor. This flow attains along-canyon speeds of over 10 m/s, with a large fraction of the canyon's depth being filled with flow at or above 5 m/s. This flow is not seen in the surface wind hodograph as it does not reach the canyon floor. Indeed, at this time, flow at the center of the landing ellipse is slightly across-canyon.

[32] At the MER landing time in the early afternoon (Figure 17b), the flow in the upper center of the canyon remains toward the east but with reduced speed. On the canyon walls, flow is now upward and out of the canyon. Maximum speeds in these ascending flows is upward of 5 m/s, with ascending motion slightly stronger on the northern wall. On the plateau surface on either side of the canyon, strong updrafts exist to a height of 10 km above the plateau surface or almost 15 km above the canyon floor. These updrafts are closed with broader and slower down-welling over the canyon, yielding a dual cell circulation over the canyon system some 240 km wide and 10 to 15 km deep. This downwelling over the canyon center tends to strongly depress the convective PBL in Melas, resulting in a PBL depth of 3 to 4 km, which is sufficiently shallow that it is below the level of the canyon rim (Figure 18). Mean winds throughout the canyon are well below 10 m/s, and there is little in the way of shear in the mean winds. On these bases, we would suggest that Melas would make a safe site for landing of the MER rovers.

[33] In the mid-evening, post sunset, strong drainage flow into the canyon returns (Figure 17c). Some of the strongest vertical winds along the wall are observed at this time on the northern wall again, attaining vertical speeds of 15 to 20 m/s. The downhill flow on either side of the canyon pours cold air into the canyon center, displacing relatively warmer air already in the canyon. This results in "gentle" (about 0.5 m/s) upwelling over a significant depth of the central canyon. The upwelling closes on the wall-hugging downwelling just above the plateau surface yielding another (now reversed) two cell flow across the canyon. Horizontal flow on the plateau is toward the west, and a strong component of the along canyon wind develops in this direction. In fact, there are two maxima in easterly flow at this time, the upper flow corresponds to extension of the plateau flow across the top of the canyon in the stratified nighttime atmosphere. The lower maximum is the channeled canyon flow. This jet of air has a sharp core and hugs the lowest elevation channel within the canyon. Winds exceed 25 m/s in this core, with flow above 15 m/s filling most of the canyon floor throughout the lowest 1 to 2 km. These strong surface-level flows predicted in the northwestward direction appear to correlate well with Mars Orbiter Camera images of streaks and dunes in the Melas Chasma (Figure 19). Thus, if high winds at night are a concern for operation of the MER rovers were a concern, Melas may be an operationally challenging landing site.

[34] The high winds in the evening at the Melas landing site results in an interesting double maxima in the convective boundary layer depth (Figure 18). The daytime maximum, with the convective PBL reaching up to 3 to 4 km above the canyon floor is thermally driven (the overturning in the PBL is driven by the buoyancy of relatively warm near-surface air heated by the ground). This is free convection and it is seen at all three landing sites. A second maximum in the convective PBL depth at Melas occurs just after 2100 LT, with the PBL depth diminishing only slowly thereafter. This second maximum in PBL convection is driven by the onset of strong, floor-level, along-canyon flow in the evening. As noted above, these winds can exceed 20 m/s at the surface, and 25 m/s in the jet core a

Figure 16. (opposite) Near-surface winds (approximately 5 m from the surface) from both of the medium-resolution mesoscale model simulations for the Melas Chasma region. (A)–(C) show the Δx = 25 km simulations, and (D)–(F) show the Δx = 5 km simulations. Four local times are plotted for each case and correspond to the local time at the center of the plotted region. (A) and (D): 0450 LT, (B) and (E): 1350 LT, and (C) and (F): 1950 LT. Background colors show local topography, with a color scale indicated below, and a scale arrow for the wind vectors is shown at the lower left.

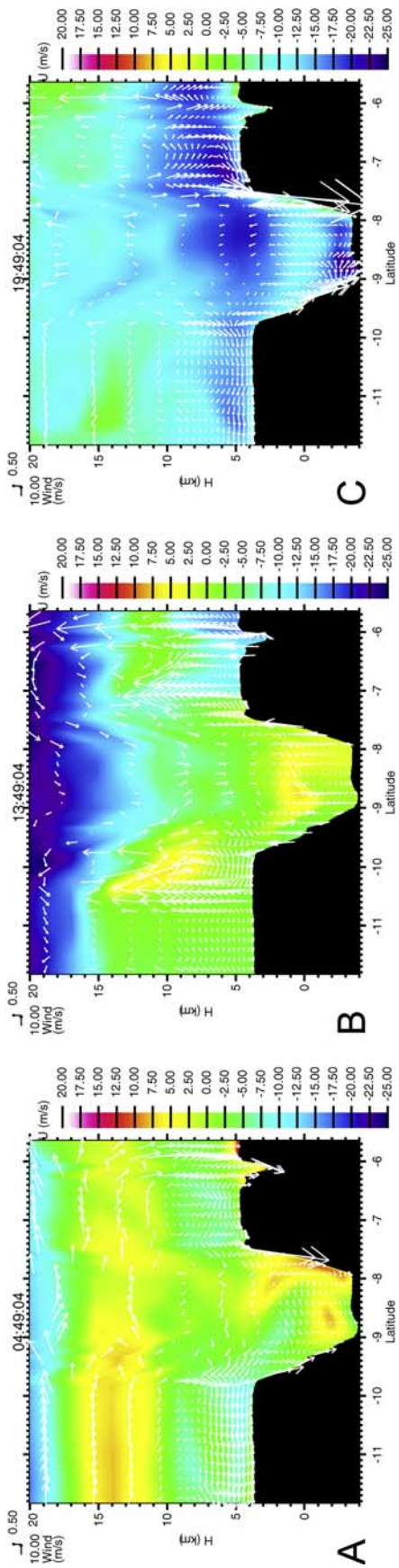

Figure 17. Winds over Melas Chasma at three sample local times of day from the $\Delta x = 5$ km simulation. The plane shown is north-south by vertical, and latitude is labeled. Background colors show the magnitude of the east-west (v) wind, and the wind vector arrows show the magnitude of the north-south and up-down winds. Since the vertical winds are much weaker than the horizontal winds, they have been exaggerated by a factor of approximately 20 relative to the horizontal component. Scale arrows for each direction are shown at the upper left of the figure. (A) 0450 LT. (B) 1350 LT. (C) 1950 LT.

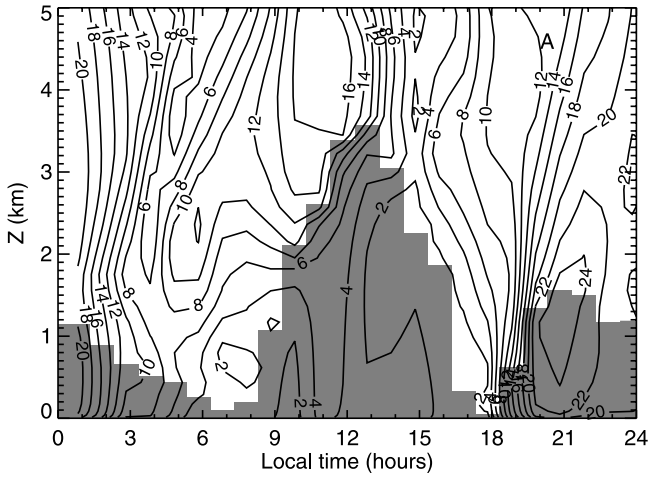

Figure 18. Plot of total horizontal wind speed as a function of local time of day and height at the proposed Melas Chasma. Wind speed is contoured in units of m/s, and the gray shading shows the Mars MM5-predicted height of the boundary layer as a function of time of day.

couple of kilometers above the canyon floor. These winds dynamically stir the boundary layer through frictional drag on surface roughness elements, despite the fact that the atmosphere is statically stability right to the surface. Hence this convection is not free; it is referred to as mechanically forced convection. The convection, and hence the depth of the boundary layer, which reaches over 1.5 km above the canyon floor, only relaxes as the regional wind patterns shift. In the hours past midnight, these winds slacken from over 20 m/s to only a few m/s, reaching less than 4 m/s by 0600 LT. At this point, the PBL depth has collapsed to only a few hundred meters.

[35] The Melas site is the furthest extrapolation of the models from the regions in which they are best tested and constrained. This is because of the strong influence of significant topography on the flow. All previous potential error sources quoted for Meridiani and Gusev still apply to Melas, but in addition, the strong along-canyon winds predicted by the model depend sensitively upon the relative importance of large-scale (tidal) winds, regional-scale (Tharsis) slope winds, and slope winds within the canyon. The model produces strongest winds at the Melas site in the evening as a result of drainage flow into the canyon within the context of regional westward flow. This regional westward flow is associated with the global scale tidal circulation, where the subsolar point leads the development of a perturbation low pressure by a few hours, which in turn leads westward (convergent) winds by a few hours. If this is the dominant system in the real atmosphere, then our prediction of the canyon wind maximum is likely in error by a few hours at most. However, the mesoscale and GCM models predict some convergent flow over the Tharsis plateau just after noon, which yields weak westward regional winds near Melas. In combination with the disruption of these regional winds at the canyon by strong upward motion at the canyon walls and the drag on mean wind in the lower atmosphere resulting from PBL convection, the model does not predict a strong jet at this time. However, if the model for some reason gets the regional-scale slope wind strengths significantly "wrong," it is not inconceivable that a canyon jet could develop in the early afternoon.

7. Summary

[36] In this paper, we have described the meteorology, and specifically the circulation and wind regimes, of three potential MER landing sites. These sites are Terra Meridiani, Gusev Crater, and Melas Chasma. In the absence of good data on near-surface winds at these sites, this study has relied on global scale (GCM) and mesoscale modeling, using the GFDL Mars GCM and the Cornell/Caltech Mars MM5. The use of poorly constrained models yields a variety of uncertainties of various magnitudes. In general, the uncertainties are larger for sites with large and varied topography, wherein interactions between global and regional circulations are complex. Generally, for any given site, while we may have high confidence that particular circulation systems will occur, predictions of wind speeds and local time of phasing are prone to error (generally a factor of a few and a few hours, respectively). Previous papers describe validation of the models used in this study against available atmospheric observations from orbiters and landers [*Wilson and Hamilton*, 1996; *Wilson and Richardson*, 2000; *Fenton and Richardson*, 2001; *Toigo and Richardson*, 2002]. The emphasis in this paper has been on providing descriptive physical interpretation of the modeled wind systems, within the context of landing safety and to provide some context for interpretation of aeolian features potentially observable at the landing sites.

[37] All three landing sites are in the tropics. As a result, the major large-scale wind systems that affect these sites are the Hadley circulation, the global tidal circulation (which also strongly modulates the Hadley circulation), and large-scale topographic circulation (which modifies both). The near-surface branch of the Hadley circulation generates a

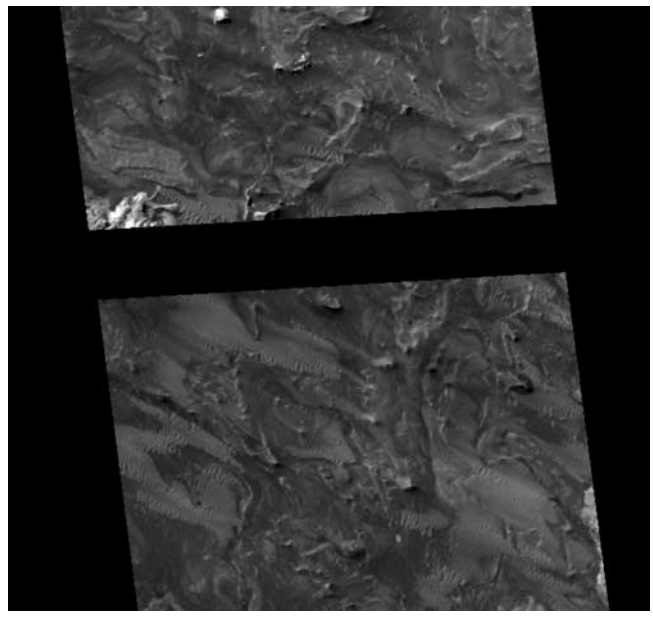

Figure 19. MOC narrow angle image showing aeolian streaks on the floor of Melas Chasma.

daily mean flow from the north to the south in the late southern summer season applicable to the MER mission. Rotation of the planet generates deflection of this flow in such a way that the wind traces a curve, with southwestward flow in the northern tropics, rotating to southeastward flow in the southern tropics. As a result of the very short radiative time constant of the atmosphere, the tropical circulation undergoes a complete rotation during the course of each day that is associated with a global pressure wave: the thermal tide (for a more technical discussion, see *Zurek et al.* [1992] and the appendix of *Wilson and Richardson* [2000]). Finally, major differences in the large-scale circulation at the three landing sites are due to regional topography. The dichotomy boundary, Elysium, and the Tharsis Plateau play important roles at one or more of the sites, by presenting obstacles to flow and/or driving large scale, thermal ''slope'' flow.

[38] The importance of local topography increases dramatically as we shift our attention from the Terra Meridiani site, to Gusev Crater, and finally to Melas Chasma. The mean winds at Terra Meridiani should be well simulated with a reasonable global scale model since the topography is relatively uniform over large distances. There is little change in the modeled mean wind as the grid spacing is decreased below about 120 km. In the Gusev region, the crater, Ma'adim Vallis and Apollinaris Patera influence flow progressively further from the landing site. For lander entry, upwelling over the crater rim and downwelling over the crater center to form a circulation cell provide the most significant deviation from the regional-scale flow. Finally, at Melas Chasma, the very deep canyon system provides a conduit for flow that channels wind along its long axis. While this can generate extremely strong (about 25 m/s) flow along the floor of the canyon at night, our simulations suggest that at the local time and location of MER landing, the along-canyon flow is much slower (only a few m/s). However, errors discussed in section 6 regarding the simulation of flow in the Tharsis region should be noted and specifically, that these errors could affect the local time phasing of peak winds.

[39] Mean winds at the tens of minutes and few kilometer scale do not provide the whole story for landing safety as they do not well represent instantaneous winds. The local time of MER landing in the early afternoon is partially responsible for the modest mean winds predicted in the model and the generally weak mean flow shear with height. However, this moderation is generated by strong momentum mixing with the ground, and the agent of that mixing is eddy turbulence. Eddy-resolving simulations at the Hematite and Gusev sites suggests that these eddies can have horizontal scales of several kilometers and vertical winds that can shift on these scales between ranges of over 7 m/s in each direction. These eddy winds may prove the most challenging aspect of the meteorology for MER descent and landing at otherwise safe and flat landing sites.

[40] The range of topography at the MER landing sites examined in this paper provides an opportunity to examine different influences on local meteorology. The global and mesoscale models suggest rich interactions of motions on scales from thousands of kilometers to hundreds of meters. Ideally, these simulations would represent the forward modeling (predictive) component of an experiment that would be closed with observations on the surface. The lack of meteorological instrumentation on MER precludes this. Although biased, we would strongly recommend carrying meteorological sensors on future landers for at least two main reasons. Such observations provide critical information that constrains our fundamental, physical understanding of how the boundary layer and small scale circulation systems on Mars operate. This is of importance for a range of scientific endeavors beyond pure meteorology, including the understanding of volatile exchange between the subsurface and atmosphere. Thus far, our observations have tended to be in flat regions without significant topographic features that could drive strong local circulations. Second, our ability to make valid predictions for future landers and aerial platforms depends strongly upon our ability to validate models. For landers, scientifically interesting sites tend to be associated with topographic complexity. Extrapolation from the current sparse observations of topographically simple sites is not guaranteed to lead to valid and consistent model predictions of complex sites. Many of the uncertainties discussed in this study could be better constrained with meteorological data of the boundary layer collected from landers in a variety of topographic and geographic locations.

[41] **Acknowledgments.** We would like to thank Richard Zurek and an anonymous reviewer for their assistance in improving this paper. This study was originally undertaken at the request of the Mars Exploration Rover mission to assist them in determining the entry, descent, and landing safety of several high-priority landing sites.

References

Dudhia, J., A nonhydrostatic version of the Penn State-NCAR mesoscale model: Validation tests and simulation of an Atlantic cyclone and cold front, *Mon. Weather Rev.*, *121*, 1493–1513, 1993.

Fenton, L. K., and M. I. Richardson, Martian surface winds: Insensitivity to orbital changes and implications for aeolian processes, *J. Geophys. Res.*, *106*, 32,885–32,902, 2001.

Golombek, M. P., et al., Selection of the Mars Exploration Rover landing sites, *J. Geophys. Res.*, *108*(E12), 8072, doi:10.1029/2003JE002074, in press, 2003.

Greeley, R., A. Skypeck, and J. B. Pollack, Martian aeolian features and deposits: Comparison with general circulation model results, *J. Geophys. Res.*, *98*, 3183–3196, 1993.

Haberle, R. M., H. C. Houben, R. Hertenstein, and T. Herdtle, A boundary layer model for Mars: Comparison with Viking Lander and entry data, *J. Atmos. Sci.*, *50*, 1544–1559, 1993.

Joshi, M. M., S. R. Lewis, P. L. Read, and D. C. Catling, Western boundary currents in the Martian atmosphere: Numerical simulations and observational evidence, *J. Geophys. Res.*, *100*, 5485–5500, 1995.

Kass, D., J. T. Schofield, T. Michaels, S. Rafkin, M. Richardson, and A. Toigo, Analysis of atmospheric mesoscale models for entry, descent, and landing, *J. Geophys. Res.*, *108*(E12), 8090, doi:10.1029/2003JE002065, in press, 2003.

Malin, M. C., and K. S. Edgett, Mars Global Surveyor Mars Orbiter Camera: Interplanetary cruise through primary mission, *J. Geophys. Res.*, *106*, 23,429–23,570, 2001.

Richardson, M. I., and R. J. Wilson, Investigation of the nature and stability of the Martian seasonal water cycle with a general circulation model, *J. Geophys. Res.*, *107*(E5), 5031, doi:10.1029/2001JE001536, 2002.

Siili, T., R. M. Haberle, J. R. Murphy, and H. Savijärvi, Modelling of the combined late-winter ice cap edge and slope winds in Mars' Hellas and Argyre regions, *Planet. Space Sci.*, *47*, 951–970, 1999.

Stevens, B., and D. H. Lenschow, Observations, experiments, and large eddy simulation, *Bull. Am. Meteorol. Soc.*, *82*, 283–294, 2001.

Stull, R. B., *An Introduction to Boundary Layer Meteorology*, Kluwer Acad., Norwell, Mass., 1988.

Toigo, A. D., and M. I. Richardson, A mesoscale model for the Martian atmosphere, *J. Geophys. Res.*, *107*(E7), 5049, doi:10.1029/2000JE001489, 2002.

Toigo, A. D., M. I. Richardson, S. P. Ewald, and P. J. Gierasch, Numerical simulation of Martian dust devils, *J. Geophys. Res.*, *108*(E6), 5047, doi:10.1029/2002JE002002, 2003.

Tyler, D., J. R. Barnes, and R. M. Haberle, Simulation of surface meteorology at the Pathfinder and VL1 sites using a Mars mesoscale model, *J. Geophys. Res.*, *107*(E4), 5018, doi:10.1029/2001JE001618, 2002.

Wang, H., M. I. Richardson, R. J. Wilson, A. P. Ingersoll, A. D. Toigo, and R. W. Zurek, Cyclones, tides, and the origin of a cross-equatorial dust storm on Mars, *Geophys. Res. Lett.*, *30*(9), 1488, doi:10.1029/2002GL016828, 2003.

Willis, G. E., and J. W. Deardorff, Laboratory observations of turbulent penetrative-convection planforms, *J. Geophys. Res.*, *84*, 295–301, 1979.

Wilson, R. J., and K. Hamilton, Comprehensive model simulation of thermal tides in the Martian atmosphere, *J. Atmos. Sci.*, *53*, 1290–1326, 1996.

Wilson, R. J., and M. I. Richardson, The Martian atmosphere during the Viking Mission, 1: Infrared measurements of atmospheric temperatures revisited, *Icarus*, *145*, 555–579, 2000.

Ye, Z. J., M. Segal, and R. A. Pielke, A comparative study of daytime thermally induced upslope flow on Mars and Earth, *J. Atmos. Sci.*, *47*, 612–628, 1990.

Zurek, R. W., J. R. Barnes, R. M. Haberle, J. B. Pollack, J. E. Tillman, and C. B. Leovy, Dynamics of the atmosphere of Mars, in *Mars*, edited by H. H. Kieffer et al., pp. 835–933, Univ. of Ariz. Press, Tucson, 1992.

M. I. Richardson, Division of Geological and Planetary Sciences, California Institute of Technology, MS 150-21, Pasadena, CA 91125, USA.

A. D. Toigo, Center for Radiophysics and Space Research, Cornell University, Ithaca, NY 14853, USA. (toigo@astro.cornell.edu)